

# DAMAGE DETECTION OF THE MAY 6, 2012 TORNADO IN TSUKUBA, JAPAN USING AERIAL THERMAL INFRARED IMAGES

Daiki HANADA<sup>\*1</sup>, Kentaro SUZUKI<sup>1</sup> and Fumio YAMAZAKI<sup>2</sup>

<sup>1</sup> Graduate student, Department of Urban Environment Systems, Chiba University,  
1-33, Yayoi-cho, Inage-ku, Chiba, 263-8522, Japan; Tel: +81-43-290-3528  
E-mail: d.hanada@chiba-u.jp; z9t0222@students.chiba-u.jp

<sup>2</sup> Professor, Department of Urban Environment Systems, Chiba University,  
1-33, Yayoi-cho, Inage-ku, Chiba, 263-8522, Japan; Tel: +81-43-290-3557  
E-mail: fumio.yamazaki@faculty.chiba-u.jp

**KEY WORDS:** Tornado, Aerial Thermal Infrared Image, Temperature Distribution, Damage Detection, GIS

**ABSTRACT:** On May 6, 2012, a strong tornado hit a part of Tsukuba City, Ibaraki prefecture, Japan. It caused heavy property damages and some human casualties in the affected area. In this study, detection of building damage was carried out from the aerial thermal infrared images taken over Tsukuba City on May 8, 2012 (two days after the tornado hit) in the daytime and nighttime. We created building footprint data and calculated the slope angle of the temperature distribution within the building footprints. It was confirmed that the temperature characteristics of non-damaged and damaged buildings show some difference. From the histogram of the average temperature within each building footprint, the average temperature for collapsed buildings was found to be in a narrower range than that of non-damaged buildings. It is expected that aerial thermal infrared images can provide useful information in early damage detection, especially at nighttime.

## 1. INTRODUCTION

On May 6, 2012, three powerful tornados were generated in Tochigi and Ibaraki Prefectures almost at the same time. These tornados caused severe property losses and some casualties although in narrow areas, such as Tsukuba City. This event was considered to be a good case to test the capability of airborne remote sensing in damage detection, especially using visible and thermal imagery. Remote sensing is widely used especially for the sites where the access from the ground is limited and the damage distribution covers wide areas (Rathje and Adams, 2008; Eguchi, 2008). Airborne remote sensing has advantages over satellite remote sensing in immediacy and applicability in cloudy conditions by flying under high clouds (Mitomi et al., 2000).

Damage detection using visible imagery is simple and easy. However, visible imagery cannot be taken in the nighttime, and thus "blank time" may occur in emergency response after a disaster strikes. On the other hand, thermal infrared (TIR) imagery can be taken both in the daytime and nighttime without depending on sunlight (Hanada and Yamazaki, 2011). Yamazaki et al. (2009) confirmed that clear edges of buildings, roads, and vegetation can be extracted from aerial TIR images of urban areas. Hanada and Yamazaki (2012) recently used ASTER's TIR images for grasping flooded areas by tsunami in the March 11, 2011 Tohoku, Japan earthquake. Satellite TIR imagery, however, has low spatial resolution, e.g. 90 m for ASTER and 60 m for Landsat-7. Hence, its application to small scale damages is difficult. However, airborne TIR imagery has much higher spatial resolution, say order of 2 to 3 m, and hence it can be used for damage detection of individual buildings, especially at nighttime when visible sensors cannot be used.

In this study, we acquired visible and TIR images from a helicopter two days after the tornado in Tsukuba City. The TIR images taken at daytime and nighttime were compared with the visible image at daytime. Visual damage inspection was first carried out using the daytime visible image by the authors for a hard-hit area of the city. The TIR images were then compared with the result of the damage inspection. The temperature distribution from the TIR images was further investigated by employing building footprints from the visible image and GIS. The temperature distribution within a footprint was compared with the damage grade of the building and the capability of aerial TIR images in damage detection was studied.

## 2. THE MAY 6, 2012 TORNADO IN TSUKUBA

A strong tornado was generated in Joso City, Ibaraki Prefecture on May 6, 2012 at 12:35. It caused significant damages along its path with 17 km in length and 500 m in width, until its end at Tsukuba City (Figure 1). The moving speed of the tornado was about 60 km/h (passing 17 km in 18 min) based on the analysis of meteorological Radar by Japan Meteorological Agency (JMA, 2012). JMA judged the Fujita scale of the tornado as F2 (the average wind speed

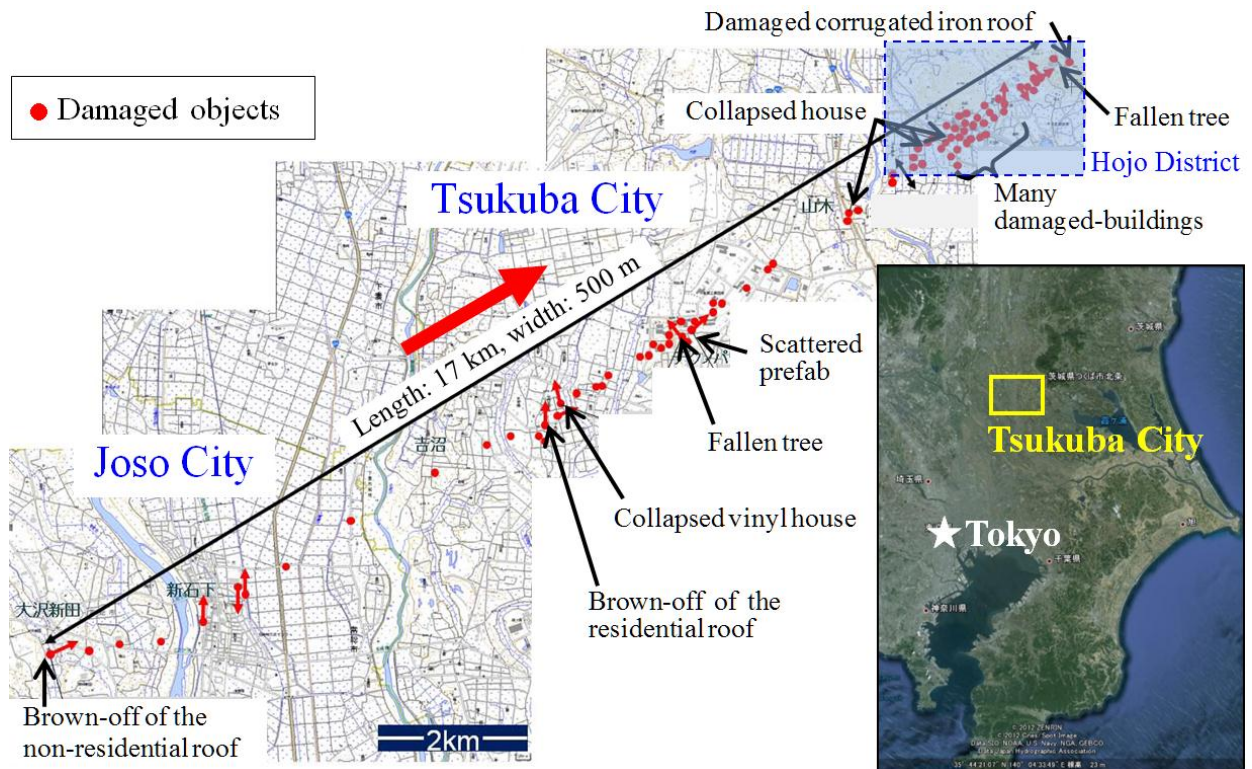


Figure 1 Detail map of the tornado's path and resultant damages, modified from JMA (2012).

of 50–69 m/s in 7 s) based on their field survey after it passed by. However, it was changed to F3 (the average wind speed of 70–92 m/s in 5 s) in June 8 because the resultant damages were found to be so severe; for example, one wood-frame house was overturned upside-down with its concrete base.

This event is ranked as one of the strongest and most damaging tornados in Japan. By this tornado, one person was killed and 37 people were injured as of May 9, 2012, and 1093 buildings were damaged as of August 31, 2012 only in Tsukuba (Tsukuba City, 2012). In the recent years, the number of strong tornados is increasing in Japan, probably due to the climate change. Prediction of the occurrence time and location of a tornado is still very difficult because its time-span is short and its affecting area is small. However, enhancement of tornado prediction, its early warning and rapid response are strongly desired to reduce human casualties due to tornados.

### 3. TIR AND VISIBLE IMAGES USED AND ANALYSIS METHOD

In this study, the detection of building damage was carried out for the tornado that hit Tsukuba City. As a study area, Hojo district, a northern part of Tsukuba City, was selected where the most serious damage was observed by the tornado (Figures 1 and 2). Assessment of building damage was carried out using by TIR and visible images taken from a helicopter of SKYMAP co. by our request after the tornado. Figures 1a and 1c show a part of the post-event visible and TIR images taken at daytime (about 14:00) on May 8, 2012 while Figure 1d shows a part of the TIR image taken at nighttime (about 19:30) on the day.

These images were taken from a small helicopter from the height of 460 m. The visible image with 0.25 m pixel size was created by mosaicing high-definition television (HDTV) scenes from a SONY handy video camera. The thermal-infrared (TIR) images with 1.54 m pixel size were mosaiced from ones taken by a TIR camera (NEC TS7302). Building footprints were created on a GIS system from the daytime aerial visible image by the present authors in order to use them in damage assessment for individual buildings.

We also conducted a field survey of Hojo district, Tsukuba City to obtain ground truth data from 14:00 to 16:00 on May 8, 2012, almost at the same time of the daytime's aerial image acquisition. Typical damages by the tornado were blown-off of buildings' roofs, broken windows, and falling-down of trees and electric poles. Since these types of damages, other than the damage to building walls, can generally be observed from vertical imagery, we thought this is a good opportunity to test the capability of aerial TIR imagery for building damage assessment as well as that of optical imagery. We surveyed the hard-hit area and look ground photos of severely damaged buildings with their GPS location data.

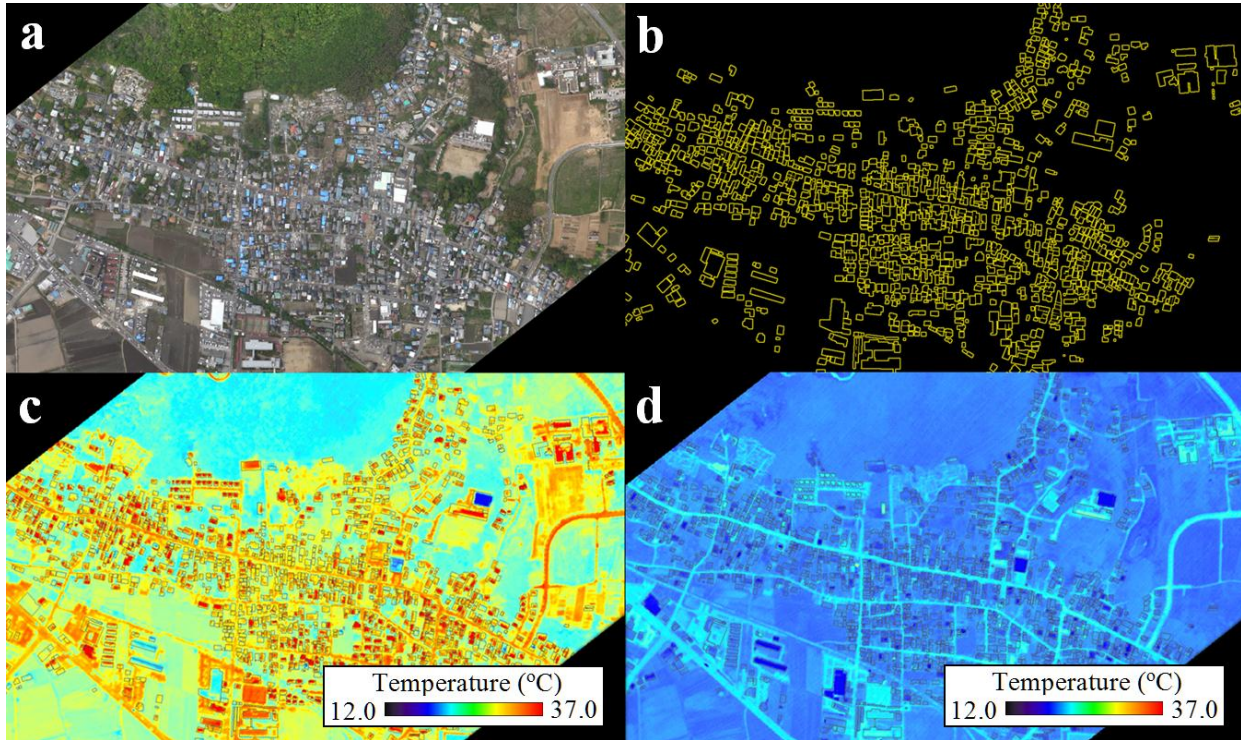

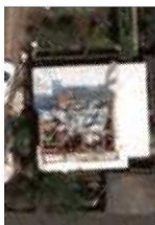




Figure 2 Visible image of Hojo district in Tsukuba City at daytime (a), building footprints created from Figure 2a (b), TIR image at daytime (c), and TIR image at nighttime on May 8, 2012 taken from helicopter.

Table 1 Damage classification to wooden houses by Cabinet Office of Japan (2009) and sample aerial photos

Damage Grade	G5	G4	G3	G2
Damage ratio of roof/floor area	$R \geq 70\%$	$50\% \leq R < 70\%$	$20\% \leq R < 50\%$	$0\% < R \leq 20\%$
Sample aerial photo				

The damage assessment was carried out in the following steps; Firstly building footprints were manually created from the daytime aerial visible image and an existing Zenrin digital map on ArcGIS software (Figure 2b). Then, damage status of each building was detected visually from the daytime aerial visible image based on the building damage classification shown in Table 1. This classification was made by Cabinet Office of Japan (2009) and it is recommended to use when evaluating the monetary loss of residential structures for local governments. In the criteria, the damage level of each wooden house is classified into 5 grades: such as no to slight (G0-G1), minor (G2), moderate (G3), major damage (G4) and collapse (G5). Out of two evaluation methods recommended, we employed the one based on the damaged floor/roof damage percentage ( $R$ ) since it is suitable to apply to vertical aerial images.

The damage level of each building was also estimated from the temperature distribution obtained from the daytime and nighttime TIR images. The average temperature and its slope angle within a building footprint were calculated and they were compared with the damage grade. The slope angle was calculated for a 3x3-pixels window (ArcGIS Resource Center, 2011). A large slope angle means a large difference in temperature between adjacent pixels while a small slope angle indicates a small difference. We considered that a severer building damage level might lead to higher variability in temperature distribution within a footprint. The average temperature within each footprint was also calculated for the daytime and nighttime TIR images using ArcGIS software. An open DXF file was generated by ArcGIS and a histogram of the average temperature for each building was made for each damage grade.

## 4. RESULTS

### 4.1 Field Survey

The route of our field survey in Hojo district on May 8, 2012 was shown by the blue line in Figure 3a. We walked around the hard-hit area with digital cameras and hand-held GPSs. The weather condition of the day was cloudy with the maximum air temperature 24.8 °C, and minimum temperature 13.4°C.

Typical damage scenes are shown in Figures 3b to 3i. Many buildings were collapsed or brown off their roofs, and these were covered by blue sheet (Figure 3b, 2h). Trees were uprooted, and a wooden house was overturned upside-down with its concrete base (Figure 3e). The Fujita scale was changed to F3 by this damage. Many objects were covered with mud because the tornado hit the area with rain (Figure 3f). This might affect the surface temperature. Debris and mud on roads were mostly cleaned up already at the time of our field survey although some still remained. Recovery efforts were very fast because the tornado damage was localized. Restoration of electric poles and cables were going on with many trucks and workers (Figure 3i).

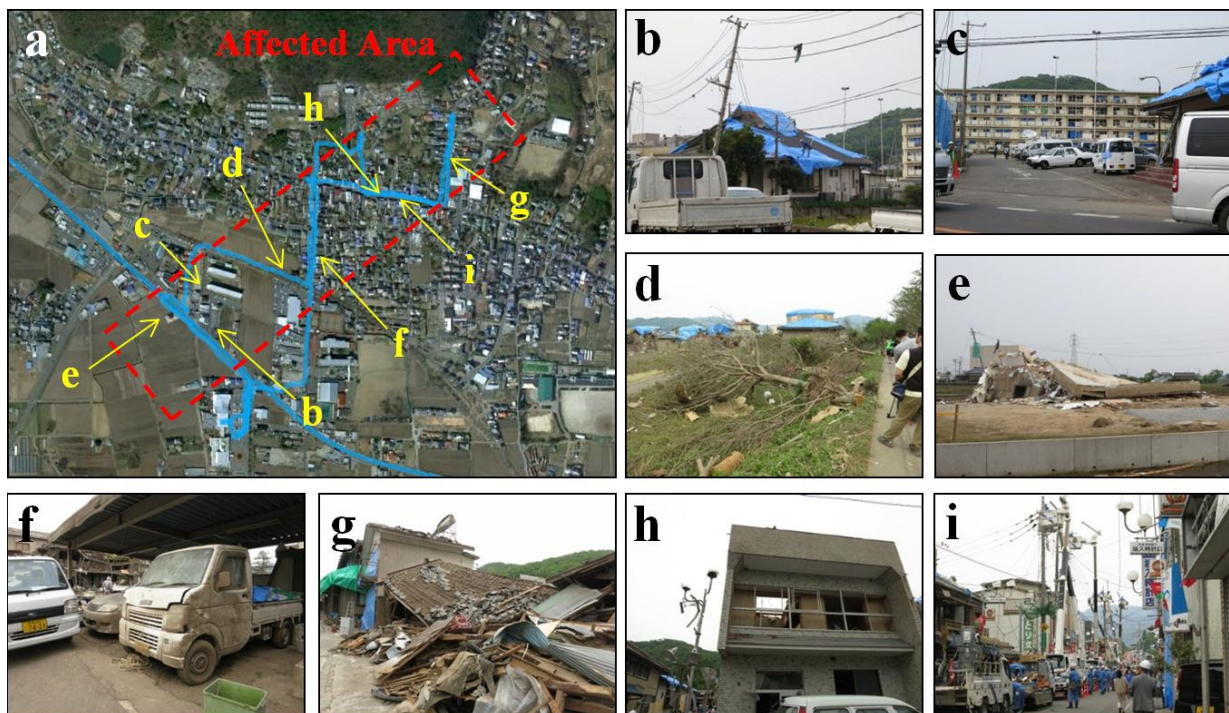


Figure 3 (a) The area of field survey in Hojo district of Tsukuba City and photo shooting locations, (b) Blue-sheet on the roof, (c) Damage on the side wall of the apartment building, (d) Fallen trees along the street, (e) Overturned wooden house with its concrete base, (f) Cars stained with tornado's mud water, (g) Buildings that reduced to debris, (h) Brown-off of the roof (the sky is seen from the window), (i) Restoration work of electric poles and cables.

### 4.2 Damage Assessment from the Post-event Visible Image

Figure 4 shows the result of our visual damage inspection from the daytime aerial visible image based on the criteria in Table 1. It is seen that the grades G3-G5 buildings were located along the path of the tornado. In this step, some buildings were judged as no damage although some damages on their side surfaces, like the apartment building in Figure 3c, because the damage was judged only from the roof condition. This might be the reason of the difference between our inspection result with the damage assessment result by Tsukuba City, as shown in Table 2. In this study, however, our inspection result was used as the reference data for the aerial TIR images since the both data were acquired from the same vertical view angle, where only the damage condition or the temperature of the roof was seen.

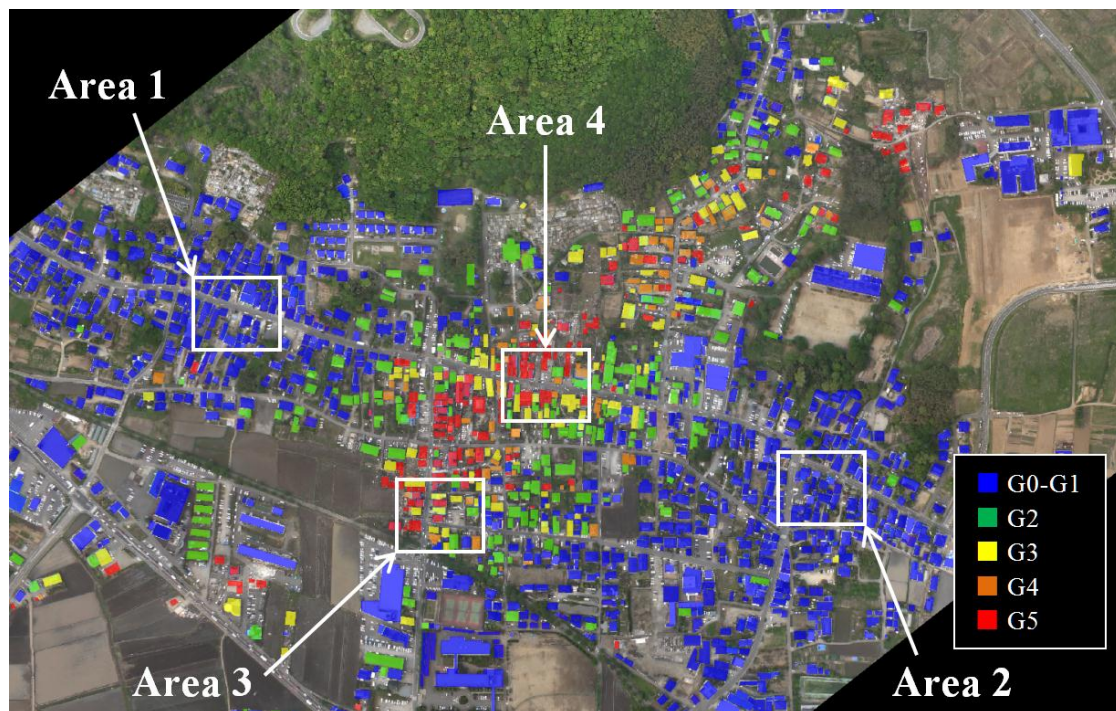


Figure 4 Damage classification result by our visual inspection of the daytime aerial visible image

Table 2 Comparison of our visual inspection result with that of Tsukuba City for Hojo district

	Tsukuba city: $T$	Visual inspection: $V$	Ratio: $V/T$ (%)
G2	373	206	55.2
G3	157	126	80.3
G4	32	43	74.4
G5	135	156	115.6
Total	697	531	76.0

### 4.3 Temperature Characteristics of Non-damaged Area from Daytime and Nighttime TIR Images

The characteristics of the TIR images at non-damaged areas were discussed first. Figure 5 show the locations of two target non-damaged areas in Figure 4. Figure 6 shows the surface temperature within the building footprints from the daytime and nighttime TIR images, superimposed on the visible image. From the daytime roof temperature distributions in Figures 6a and 6c, the roofs mostly show high temperature although some low temperature roofs exist. From the nighttime roof temperature distributions in Figure 6b and 6d, the buildings showing high temperature at daytime are still in relatively higher temperature at nighttime. It is observed that the roof temperature within a footprint of a non-damaged is mostly uniformly distributed but the effects of surrounding vegetation, shadow and footprint's accuracy can be observed around the outline.

Figure 7 shows the slope angle of the surface temperature within the footprints. In calculation of the slope angle, the temperature of the adjacent pixels affected the result although the angle is shown only within the footprints. In the daytime slope angles in Figures 7a and 7c, high temperature roofs show generally larger slope angles because the temperature difference with their surroundings is large due to the difference of surface materials. In the nighttime slope angles in Figure 7b and 6d, the slope angles within some building outlines are displayed red color affected by surrounding road or vegetation. However most building roofs are in low temperature with uniform distribution, and thus their temperature change within its outline is small.



Figure 5 Target areas of non-damage in Figure 4.

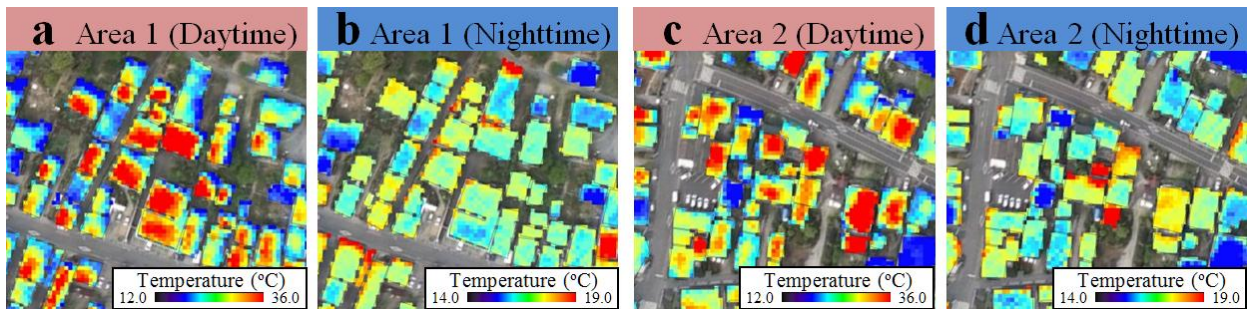


Figure 6 Temperature within building footprints for non-damage areas, **a, c**: Daytime, **b, d**: Nighttime.

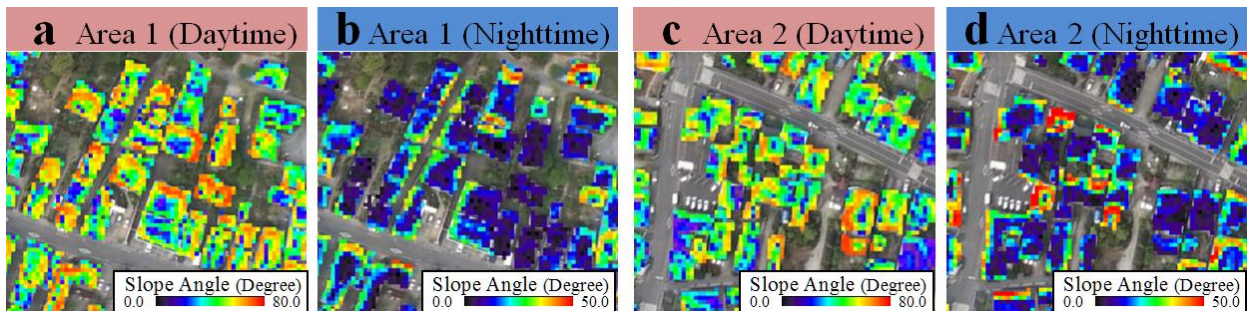


Figure 7 Slope angle of the temperature within building footprints in Figure 6, **a, c**: Daytime, **b, d**: Nighttime.

#### 4.4 Temperature Characteristics of Heavy-damage Areas from Daytime and Nighttime TIR Images

Next the characteristics of the TIR images at heavily-damaged areas were discussed. Figure 8 show the locations of two target heavily-damaged areas in Figure 4. Figure 9 shows the surface temperature within the building footprints from the daytime and nighttime TIR images, superimposed on the visible image. From the daytime roof temperature distributions in Figures 9a and 9c, damaged roofs mostly show low temperature because they were covered by blue sheet or reduced to debris. The nighttime roof temperature distributions in Figure 9b and 9d also exhibit low values. The temperature distributions for heavily-damaged buildings are seen to be somewhat different from those of non-damaged ones both at daytime and nighttime, but this observation is highly affected by the material, color and orientation of the roof, shadow and surrounding conditions.

Figure 10 shows the slope angle of the surface temperature within the footprints. In the daytime slope angles in Figures 10a and 10c, many buildings show small values as in purple to blue colors. It is also observed that the pixels with large angles are few probably because buildings were reduced debris and it spread in and outside of the original building footprints. Many materials were mixed up by building collapse and thus many objects became a mixed-pixel (mixel) condition for the low resolution TIR images (1.54m). This characteristic is remarkable especially for the upper left building group in Figure 10b. Most footprint areas show small changes as in dark blue color. It can be seen in the visible image of Area 3 that the spread debris in the area became the similar condition as soil. This kind of debris spread was also observed in our field survey, and hence there is possibility to use this more uniform temperature distribution with the surroundings in early damage detection from TIR images.



Figure 8 Target areas of heavy-damage in Figure 4.

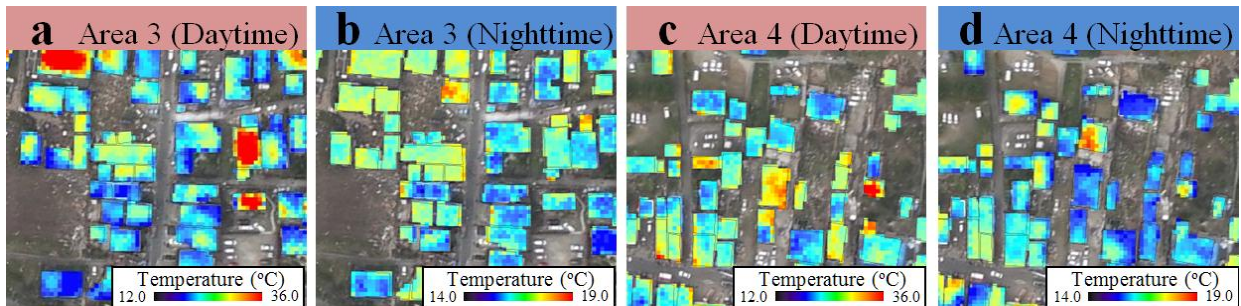


Figure 9 Temperature within building footprints for heavy-damage areas, **a, c**: Daytime, **b, d**: Nighttime.

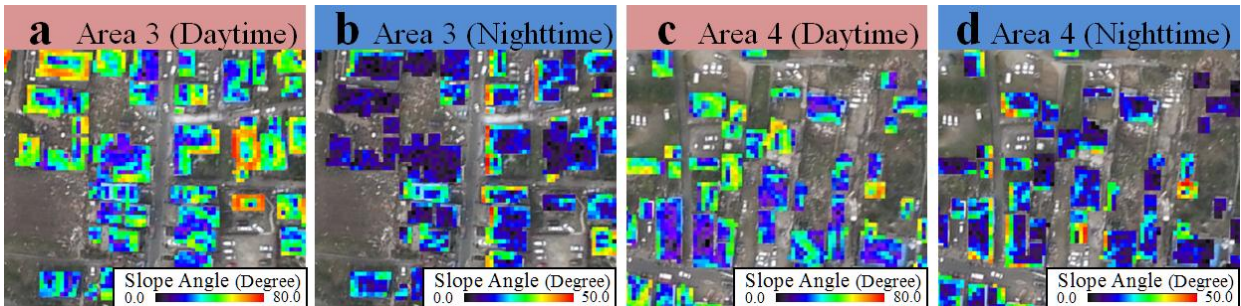


Figure 10 Slope angle of the temperature within building footprints in Figure 9, **a, c**: Daytime, **b, d**: Nighttime.

#### 4.5 Histogram of Average Temperature within Footprint for Each Damage Level

Figure 11 shows the histograms of the average temperature within building footprints for each damage level and Table 3 shows the number of buildings for the five damage levels. Note that buildings other than in Hojo district are also counted in this section.

From the daytime histogram in Figure 11a, the average roof temperatures for non-damaged buildings are seen to be widely distributed in the range from 20 to 40 °C. On the contrary, those for damaged buildings are displayed in a narrower range from 24 to 35 °C and the range gets small as the damage level gets higher. For collapsed buildings (G5), the average temperature becomes in the range from 25 to 33 °C. This is because that the roofs were lost and the footprint areas were covered by the mixture of various materials like debris and mud. If we can use a much higher-resolution TIR image, a wider temperature distribution can be seen in more detail. But at this time, the resolution of our TIR images are 1.54 m, and thus most debris became in a mixel condition and the temperature distributions became flat. The histogram for damaged buildings at daytime tends to be in a narrow range and the average values were decreased for 2 or 3 °C.

From the nighttime histogram in Figure 11b, the average temperatures for most buildings are seen in narrower ranges, around 17 °C, compared with the daytime histograms, as typically observed for collapsed buildings (G5). The histograms for damaged buildings at nighttime also tend to be in narrower ranges, the same as the daytime case. This kind of temperature characteristics in aerial TIR images may be used in early damage detection in the future although more examples for various conditions should be tested.

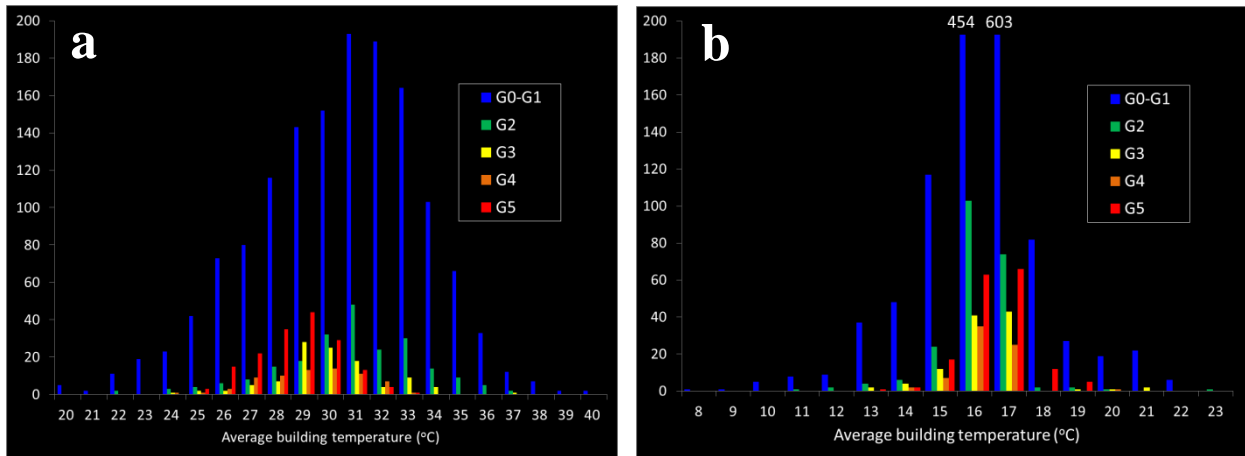


Figure 11 Histogram of average temperature within footprint for each damage level, a: Daytime, b: Nighttime.

Table 3 Number of buildings in each damage level

	G0-G1	G2	G3	G4	G5
Number of Buildings	1440	220	106	70	166

## 5. CONCLUSION

In this study, aerial thermal infrared images were used to grasp building damages caused by the tornado that hit Tsukuba City, Japan on May 6, 2012. We acquired visible and TIR images over Hojo district of the city from a helicopter two days after the tornado struck. First building footprint data were created manually from the acquired visible image and the existing GIS map. Visual damage inspection was then carried out using the daytime visible image for a hard-hit area of the city. The TIR images were then compared with the result of the damage inspection. The temperature distribution within the footprints was further investigated on a GIS.

From the average temperature distribution within non-damaged and damaged-building footprints, non-damaged buildings showed higher temperatures with a larger range than those of damaged-buildings. This observation may be explained by the fact that due to the mixture of various materials at the collapsed roof location, the temperature was generally reduced. The change of temperature within each footprint was also evaluated using the slope angle of the temperature. But the slope angle was also strongly affected by the temperature itself, and a clear trend was not found for damaged buildings.

From the histograms of the average temperature within building footprints for five damage levels, that for the collapsed level was distributed in a narrower range than that for non-damaged one's both at daytime and nighttime. The temperature distribution was seen to become flat as the damage level goes up. This is due to the mixed-pixel of debris and others around the original footprint, especially for the low spatial-resolution TIR images used in this study.

We tested the aerial TIR images after the tornado in this study since TIR imagery can be obtained even at nighttime and thus is possible to reduce "blank time" after a disaster strikes. However, due to the limitation of its spatial resolution, about 1.5 m in the current example, it was not so easy to detect small damage to individual buildings. Another important drawback of TIR imagery is that it is highly affected by the roof material, color and its orientation as well as the surrounding condition and the weather and air-temperature. More case studies are necessary in the future to utilize aerial TIR imagery for early damage detection after a disaster strike, especially at nighttime.

## REFERENCES

- ArcGIS resource center, 2011. How Slope Works, <http://help.arcgis.com/en/arcgisdesktop/10.0/help/index.html#/na/009z000000vz000000/>
- Cabinet Office of Japan, 2009. Operational Guidelines of Damage Certification Criteria for Residences (in Japanese) URL: <http://www.bousai.go.jp/hou/pdf/shishinall.pdf>
- Eguchi, R.T., Huyck, C., Ghosh, S., and Adams, B.J., 2008. The Application of Remote Sensing Technologies for Disaster Management, the 14th World Conference on Earthquake Engineering, CD-ROM.
- Hanada, D., and Yamazaki, F., 2011. Detection of the Flooded Area by Tsunami Using Satellite Thermal Infrared Images, the 32nd Asian Conference on Remote Sensing, Paper No. 229, CD-ROM, 6p.



- Hanada, D., and Yamazaki, F., 2012. Detection of Flooded Areas by the Tohoku Earthquake/tsunami Using ASTER Thermal Infrared Images, 9th International Conference on Urban Earthquake Engineering & 4th Asia Conference on Earthquake Engineering, Tokyo Institute of Technology, Tokyo, Japan, CD-ROM, 235-239.
- Japan Meteorological Agency, 2012. Report of the Tornado Occurred on May 6, 2012 (in Japanese).  
URL: <http://www.jma.go.jp/jma/press/1206/08b/toppu120608.html>
- Mitomi, H., Yamazaki, F., and Matsuoka, M. 2000. Automated Detection of Building Damage due to Recent Earthquakes using Aerial Television Images and Photographs, Proc. of the 21st Asian Conference on Remote Sensing, Vol. 1, 401-406.
- Rathje, E, and Adams, B.J., 2008. The Role of Remote Sensing in Earthquake Science and Engineering, Opportunities and Challenges, Earthquake Spectra, 24(2), 471–492.
- Tsukuba City, 2012. Damage Situation by the Tornado Occurred on May 6, 2012 (in Japanese).  
URL: [http://www.city.tsukuba.ibaraki.jp/dbps\\_data/\\_material\\_/localhost/kou002/tatsumaki/No149.pdf](http://www.city.tsukuba.ibaraki.jp/dbps_data/_material_/localhost/kou002/tatsumaki/No149.pdf)
- Yamazaki, F., Murakoshi, A., and Sekiya, N., 2009. Observation of Urban Heat Island using Airborne Thermal Sensors, 2009 Urban Remote Sensing Joint Event, IEEE, Shanghai, China, CD-ROM.